

Transition to Saltatory Conduction

**The “Lillie Transition”: Models of the Onset of Saltatory Conduction in Myelinating Axons**

Robert G. Young, Ann M. Castelfranco and Daniel K. Hartline

Békésy Laboratory of Neurobiology  
Pacific Biosciences Research Center  
University of Hawai`i at Manoa  
Honolulu, HI 96822

RUNNING HEAD: Transition to Saltatory Conduction

CORRESPONDING AUTHOR: Ann M. Castelfranco  
Pacific Biosciences Research Center  
1993 East-West Rd.  
Honolulu, HI 96822  
castelf@pbrc.hawaii.edu  
phone: (808) 956-9283  
FAX: (808) 956-6984

### **Abstract**

Almost 90 years ago, Lillie reported that rapid saltatory conduction arose in an iron wire model of nerve impulse propagation when he covered the wire with insulating sections of glass tubing equivalent to myelinated internodes. This led to his suggestion of a similar mechanism explaining rapid conduction in myelinated nerve. In both their evolution and their development, myelinating axons must make a similar transition between continuous and saltatory conduction. Achieving a smooth transition is a potential challenge that we examined in computer models simulating a segmented insulating sheath surrounding an axon having Hodgkin-Huxley squid parameters. With a wide gap under the sheath, conduction was continuous. As the gap was reduced, conduction initially slowed, owing to the increased extra-axonal resistance, then increased (the “rise”) up to several times that of the unmyelinated fiber, as saltatory conduction set in. The conduction velocity slowdown was little affected by the number of myelin layers or modest changes in the size of the “node,” but strongly affected by the size of the “internode” and axon diameter. The steepness of the rise of rapid conduction was greatly affected by the number of myelin layers, and axon diameter, variably affected by internode length and little affected by node length. The transition to saltatory conduction occurred at surprisingly wide gaps and the improvement in conduction speed persisted to surprisingly small gaps. The study demonstrates that the specialized paranodal seals between myelin and axon, and indeed even the clustering of sodium channels at the nodes, are not necessary for saltatory conduction.

**Keywords:** Myelin, Evolution, Conduction velocity, Axon, Nodes of Ranvier, Computational modeling

### 1 Introduction

In 1925, Ralph Lillie discovered the mode of action of myelin (Lillie 1925). He had been studying a model of nerve impulse conduction consisting of an iron wire immersed in nitric acid, which when electrically or mechanically activated, triggered an electrochemically-mediated local breakdown and reestablishment of the nitrate coating that propagated along the wire much as occurs in unmyelinated nerve. Lillie was investigating the changes in conduction velocity brought about by enclosing the wire in a glass tube to increase the resistivity of the current-return path through the external medium. In these studies, he documented the slowdown of conduction with the tightening of the “periaxonal” space and established the square root relationship between external conductivity and velocity, now accepted for real nerve fibers. He further discovered that when he threaded short insulating segments of glass tubing along his iron wire, the “impulse” conduction transitioned to a more rapid “saltatory” mode. This led to his prescient suggestion of a similar mechanism as the explanation for the rapid conduction in myelinated nerve, which was confirmed in physiological experiments by Tasaki (1939) and later, by Huxley and Stämpfli (1949). We will thus refer to such a transition of conduction mode as the “Lillie Transition.”

A similar transition from continuous to saltatory conduction occurred in the evolution of myelin from preexisting non-myelinated nervous systems, and indeed, it routinely happens in normal nervous system development. Vertebrates that have little if any myelin at birth or hatching myelinate their originally continuously-conducting axons through a significant portion of postnatal existence (e.g. Carpenter and Bergland 1975; Foster *et al.* 1982; Vabnick and Shrager 1999, Brösamle and Halpern 2002), and axons in myelinate invertebrates also transition from unmyelinated to myelinated in the course of development (Xu *et al.* 1994; Wilson and Hartline 2011). Its occurrence in evolution is exemplified by the myelinated dorsal giant axons of shrimp, which have unmyelinated presumed homologues in the more basal Malacostraca (Freidländer 1889), and the myelinated Mauthner cells of fish, which are unmyelinated among the lampreys (Rovainen 1967). The changeover between unmyelinated and myelinated states has major consequences for the operational characteristics of the nervous system (e.g. changes in feedback loop and delay-line timing, muscle synchrony, etc; Seidl *et al.* 2010; Wilson and

## Transition to Saltatory Conduction

Hartline 2011), as well as potential difficulties to be surmounted for a smooth transition. It is not altogether clear how smooth such a transition might be under various assumed conditions, since abrupt changes in electrical properties in an axon (among which conduction mode might be included) can lead to spike failure or reflections (Goldstein and Rall 1974; Calvin and Hartline 1977). We thus studied the behavior of computer models that paralleled the experimental set up utilized by Lillie, examining the interplay of continuous and saltatory conduction across the Lillie transition using the more physiological model provided by Hodgkin-Huxley type active properties in axons (rather than iron wires) surrounded by sheaths possessing the key electrical properties of myelin (Hodgkin and Huxley 1952; Halter and Clark 1991; Hines and Shrager 1991). This approach provides a convenient framework for examining the acquisition of saltatory conduction with myelination, since the change in conduction mode can be achieved by varying only one parameter – the tightness of the insulating sheath, which is analogous to adding segments of insulating glass tube to the iron wire in Lillie's model. We have attempted thereby not only to bridge the seminal observations of Lillie with more realistic physiology, but also to gain insight into developmental and evolutionary constraints on the acquisition of a saltatory mode of impulse conduction. We show that conditions for achieving saltatory conduction are quite permissive, but that improvement in those conditions can lead to increased performance (conduction velocity) over a large range.

## 2 Methods

Axon models were constructed in the NEURON simulation environment of Hines, Moore and Carnevale (Carnevale and Hines 2005). The models, diagrammed in Fig. 1, simulated a central active core conductor representing an unmyelinated axon (in place of a nitric-oxide-coated iron wire) surrounded by a sheath. The sheath was constructed to simulate the multiple layers of a myelin coat, and was punctuated by breaks corresponding to the breaks between Lillie's glass tube sections, leaving only the unmyelinated axon in the simulated nodes between sheath/tube sections. NEURON's default squid axon kinetics were used for our unmyelinated base axon. The axial specific resistance ( $R_i$ ) and specific membrane capacitance ( $C_m$ ) were set to 35.6  $\Omega$  cm and 1  $\mu$ F cm<sup>-2</sup>, respectively. Hodgkin-Huxley default squid values were used for maximum specific sodium and potassium conductances: 0.120 S cm<sup>-2</sup> and 0.036 S cm<sup>-2</sup>,

## Transition to Saltatory Conduction

respectively and a leak conductance of  $0.0003 \text{ S cm}^{-2}$  (Hodgkin and Huxley 1952). Simulations were run at the default temperature of  $6.3 \text{ }^\circ\text{C}$  unless otherwise specified. As was the case for the active process in Lillie's iron wire model, our more physiological ionic mechanisms were distributed uniformly along the entire axon, in the axolemma of internodal as well as nodal regions. Thus there was never a case of impulse failure, as there was always an impulse conducted in the submyelin space. NEURON's "extracellular" mechanism was used to surround the  $10 \text{ }\mu\text{m}$  diameter base axon with the segmented "myelin" sheath of high resistance and low capacitance. Short stretches lacking the sheath simulated nodes (101 nodes per axon) so the nerve fiber consisted of alternating nodal and internodal sections. The base fiber had nodes of length ( $L_n$ )  $10 \text{ }\mu\text{m}$ , which yielded a channel number in the nodal section in the range of 90,000 channels, the same order of magnitude (*ca.* 60,000) reported for vertebrate nodes (Hille 1992). The base "myelin" sheath segment lengths ( $L_s$ ) were  $1500 \text{ }\mu\text{m}$  and were enclosed in the equivalent of 100 wraps ( $nl$ ) of double-membrane insulation -- similar to myelinated vertebrate nerves (Raine 1984). Each wrap effectively added two resistors ( $10^6 \text{ }\Omega \text{ cm}^2$  each) and two capacitors ( $1 \text{ }\mu\text{F cm}^{-2}$  each) in series to the internodal sections. The result was that for a sheath possessing  $nl$  wraps, sheath conductance and capacitance were  $1/R_s = (10^{-6})/(2nl) \text{ }\Omega \text{ cm}^2$  and  $C_s = 1/(2nl) \text{ }\mu\text{F cm}^{-2}$ , respectively. Between the extracellular sheath and the axon core was a submyelin space, the width of which will be termed the "submyelin gap",  $\delta$ . The longitudinal resistance of the submyelin space was set to  $R_o = 35.6/A \text{ }\Omega \text{ cm}^{-1}$ , where  $A$  is the cross-sectional area in  $\text{cm}^2$  of the submyelin space. Our model excluded specialized structures at the paranodes, which were not present in Lillie's analog model and which we further may reasonably assume develop later in evolution. The primary independent variable studied was the submyelin gap,  $\delta$ , its effect on conduction velocity and its value at the "Lillie transition" to saltatory conduction. Values of  $\delta$  examined were routinely varied from  $1 \text{ nm}$  to  $100 \text{ }\mu\text{m}$ , which range includes the width of submyelin space in vertebrate axons ( $10 - 20 \text{ nm}$ ) and extended to large enough values to simulate in effect an unmyelinated axon. A series of runs over this range of  $\delta$  was made separately for each of four parameters governing fiber geometry, as diagrammed in Fig. 1. These were the number of myelin layers ( $nl$ ), the length of the nodes ( $L_n$ ), the length of the internodes ( $L_s$ ) and the axon diameter, with the parameter range for each given in Table 1.

## Transition to Saltatory Conduction

The numerical simulation of a fiber used NEURON's default backward Euler integration method with fixed time steps of  $dt = 12.5 \mu\text{s}$ . Smaller  $dt$  values significantly increased runtime while changing computed conduction velocity by less than 1% for the range of myelin parameters we examined. Each nodal and internodal section was divided into a number ( $nseg$ ) of numerical compartments of equal length; and calculations were done at the midpoint of each compartment and the endpoints of each section. Odd integer  $nseg$  values were chosen for each section to ensure that computations referred to the midpoints of each section. Preliminary simulations showed that errors in conduction velocity occurred in some neurons with large compartment sizes (large section lengths with low  $nseg$  values). Dramatic errors occurred in the form of conduction failure in neurons with small  $\delta$  sizes, long internodal lengths, and low  $nseg$  values. Thus for sections shorter than  $10 \mu\text{m}$  in length,  $nseg$  values were chosen to ensure that the length of each numerical compartment was about  $1 \mu\text{m}$ . The  $nseg$  values were chosen to give compartment lengths between  $1 \mu\text{m}$  and  $3 \mu\text{m}$  for sections of length  $10 \mu\text{m}$  to  $1500 \mu\text{m}$ , and about  $3 \mu\text{m}$  for sections longer than  $1500 \mu\text{m}$ . Further increasing the  $nseg$  values significantly increased computer runtime while altering computed conduction velocity by less than 1% for the fiber parameter-ranges covered.

Suprathreshold stimuli were applied at one (sealed) end of the fiber. Action potentials were recorded near the center of the fiber to avoid artifacts due to end effects and stimulation current, and to ensure that the traveling voltage waves were in steady state. Conduction velocities were calculated by monitoring the voltage activity at the center of the 40th and 60th nodes. Conduction velocity was defined as the distance between the centers of those two nodes divided by the time difference in impulse occurrence between them. Impulse occurrence was determined by the first crossing by the voltage-trajectory of a pre-determined level. For *conduction velocity* calculations this criterion voltage was  $-35 \text{ mV}$ , and the time of occurrence was determined by interpolating the time between adjacent voltage points spanning this level. Since voltage was measured at corresponding points in the two nodes, the impulse had the same shape at both, so the criterion was independent of the specific impulse shape. For determining the occurrence of *saltatory conduction*, however, the zero-crossing of the voltage was chosen, being a voltage that seemed relatively unperturbed by complexities in spike shape that accompanied the impulse trajectories at other voltages. Saltatory conduction was thus deemed to

## Transition to Saltatory Conduction

occur when the impulse at a more “distal” or “downstream” node crossed  $V = 0$  mV prior to the  $V = 0$  mV crossing of the impulse traveling in continuous mode under the myelin.

### 3 Results

#### 3.1 Transition to saltatory conduction is preceded by a slowdown in conduction velocity

When the axon was surrounded by a sufficiently loose sheath, it conducted in a continuous or incremental fashion, as did Lillie’s iron wire. As the sheath, punctuated at intervals by breaks representing the nodes of Ranvier was tightened, a transition occurred in which a rapid, saltatory conduction mode of impulses jumping from node to node was added to the slow continuous conduction still occurring in the submyelin spaces. This is illustrated in Fig. 2, which presents plots of conduction velocity as a function of the submyelin gap,  $\delta$ , on a logarithmic scale for three different temperatures within the natural environmental range for squid. Here,  $\delta$  ranges from 100  $\mu\text{m}$ , representing an effectively unmyelinated axon, down to 0.001  $\mu\text{m}$ , representing a tightly-wrapped sheath of a myelinated axon ( $\delta = 0$   $\mu\text{m}$  results in a singularity). The basic model behavior for two distinct cases at  $\delta = 0.01$  and 10  $\mu\text{m}$  are shown in the two insets to Fig. 2, which plot three “snap shots” at 1.25 ms intervals of the trans-fiber voltage as a function of position along the fiber.

At  $\delta = 10$   $\mu\text{m}$ , conduction velocity in our standard “base” axon (6.3°C: black line) was 1.73  $\text{m s}^{-1}$ , and signal propagation was found to be only continuous, with a static waveform (a time-invariant longitudinal profile) propagating down the length of the axon (Fig. 2, lower inset). As the sheath was tightened, i.e.  $\delta$  was decreased to 1.6  $\mu\text{m}$ , conduction velocity steadily dropped to a minimum of 1.60  $\text{m s}^{-1}$ . This 8% decrease can be attributed to the increased resistance in the extracellular submyelin current-return path as described by Lillie (1925). Further decreasing  $\delta$  below 1.6  $\mu\text{m}$  resulted in a reversal in the downward trend followed by a steep but not discontinuous increase in conduction velocity, along with a significant change in the behavior of signal propagation: “saltatory” conduction. With this tighter  $\delta$  value, nodal membrane began firing impulses before the arrival of the continuously-propagating submyelin impulses, the reverse of the situation in continuous conduction. Impulses still propagated in continuous mode

## Transition to Saltatory Conduction

beneath the myelin but instead of traveling orthodromically in the same direction (which for convenience we will refer to as “proximal” to “distal”) they spread in both directions from each node, the two oppositely-propagating impulses of a given internode meeting and annihilating in mid-internode. The same effect was reported by Lillie (1925) in his iron wire model. With further tightening, the firing of nodes (abrupt corners in the waveform of Fig. 2, upper inset) became progressively more pronounced, with the voltage profiles along internodes becoming piecewise linear segments connecting adjacent node values but following a spatial trajectory representing the same shape. The piecewise linearity can be understood as resulting from the ohmic voltage drop along the longitudinal axoplasmic resistance that is surrounded by a current-blocking sheath. The result was a waveform of the same duration that propagated faster. It was expanded in proportion to the increased conduction velocity, and was more “dynamic,” in that the shape of the impulse, being piecewise linear and only approximating a smooth action potential, changed progressively over the time span it took the impulse to travel between successive nodes (see Goldman and Albus 1968 for a version of this behavior with different myelin and nodal channel parameters). With further sheath tightening beyond the transition point, conduction velocity continued to rise, reaching  $9.4 \text{ m s}^{-1}$  for  $\delta = 0.001 \text{ }\mu\text{m}$ , as shown in Fig. 2 and plateauing at around  $15 \text{ m s}^{-1}$  for very tight sheaths ( $\delta < 10^{-6} \text{ }\mu\text{m}$ ).

As the temperature increased to 10.0 and 15.0 °C (gray lines in Fig. 2), slight changes occurred in the behavior of our model axon. First, the unmyelinated velocities at  $\delta = 10 \text{ }\mu\text{m}$  were 14.3% and 34.5% higher at 10.0 and 15.0 °C, respectively, than at 6.3 °C. As the submyelin gap decreased, conduction velocity dropped 10.1% and 19.5% from the unmyelinated velocity at 10.0 and 15.0 °C respectively—compared to 8% at 6.3 °C—before speeding up. As  $\delta$  tightened to 0.001  $\mu\text{m}$ , velocities of axons at 10.0 and 15.0 °C increased 450% and 453% higher than their respective unmyelinated velocities—compared to 442% at 6.3 °C. Thus, the changes in conduction velocity with  $\delta$  were all qualitatively conserved and quantitatively little altered over the naturally-occurring temperature range within which squid and many other marine ectotherms normally function, and myelin may be assumed to have evolved (Hartline and Coleman 2007; Zalc *et al.* 2008).



## Transition to Saltatory Conduction

The influence of characteristics of the fiber geometry such as sheath thickness, node length, internode length or axon diameter, on the relationship between conduction velocity and sheath tightness ( $\delta$ ) is examined in Fig. 3, which presents a series of 3D graphs in which velocity ( $v$ ) is plotted on the vertical ( $z$ ) axis,  $\delta$  is varied along the  $x$  axis, and a property of the fiber geometry is varied along the  $y$  axis. The same trend of velocity dependence on  $\delta$  was consistently present in all cases: initially, as  $\delta$  decreased, the conduction velocities also decreased owing to the increased submyelin resistance. This trend then reversed, and conduction velocity rose, approaching a maximum as the gap disappeared (an asymptotic approach to a plateau seen, e.g., for small numbers of myelin layers in the semi-log plots of Fig. 3A2). In the range of relatively large gaps where conduction velocity slowed, the impulse only propagated in a continuous mode under the myelin. For each set of studies, there was a  $\delta$  that yielded a minimum velocity,  $\delta_{slow}$ , which was denoted by a white dot with centered black star on the graphs. Further reduction of  $\delta$  resulted in a slight increase in conduction velocity just prior to the transition to a saltatory mode of propagation (this transition will be examined in more detail in section 3.6). The largest submyelin gap tested that sustained saltatory conduction, denoted by “ $\delta_{salt}$ ”, was considered to correspond to the submyelin gap of the Lillie transition. Results reported below were qualitatively independent of temperature within the natural range (6.3 – 15.0 °C).

### 3.2 Sheath thickness strongly affects rising phase but not slowdown or Lillie transition

The influence of sheath thickness on the Lillie transition is shown in Fig. 3 panels A1-A3. The left panel (Fig. 3A1) is the 3D plot, with the number of double layers ( $nl$ ) in the sheath represented along the right horizontal ( $y$ ) axis. Panels A2 and A3 show sections through the surface in the  $\delta$ - $v$  ( $x$ - $z$ ) and  $nl$ - $v$  ( $y$ - $z$ ) planes for specific values of the third variable,  $nl$  or  $\delta$ , respectively. Since the most significant effect of myelin arises from its capacitance-reduction properties, it is expected that the number of wraps (the thickness of the myelin) will have a strong influence on conduction velocity. As shown in Fig. 3A2, when the number of wraps ( $nl$ ) was small, conduction velocity was only modestly  $\delta$  dependent on the submyelin space size,  $\delta$ . Thus, with  $nl = 1$ , varying  $\delta$  over the range from 10  $\mu\text{m}$  to 1 nm only resulted in a velocity variation of 0.25  $\text{m s}^{-1}$  or 14% around the 1.73  $\text{m s}^{-1}$  of the unmyelinated case (solid black line in

## Transition to Saltatory Conduction

Fig. 3A1 and 3A2). With just this single wrap, a form of saltatory conduction still occurred, as defined in Methods, but behavior differed from that seen with multiple wraps in ways that are beyond the scope of the present report. With  $nl = 300$ , conduction velocity varied by  $8.85 \text{ m s}^{-1}$ , more than a 5-fold change over the same  $\delta$  range (white line with black dashes in Fig. 3A1 and 3A2). When  $\delta$  is large, conduction velocity is (trivially) independent of all of the other myelin parameters, including  $nl$ , since conduction is that of an unmyelinated axon. Thus, for  $\delta = 10 \text{ }\mu\text{m}$ , with  $nl$  running from 1 to 300, conduction velocity changed only 0.1% (black line with white dashes in Fig. 3A1 and 3A3). However, when  $\delta$  was reduced to 5 or 1 nm, velocity rose 289% and 467%, respectively, over the same range of  $nl$  (lightest gray line with white dashes and solid white line, respectively, in Fig. 3A1 and 3A3). In contrast, but almost equally obviously, the submyelin gap yielding the minimum velocity,  $\delta_{slow}$ , and the corresponding decrease in conduction velocity was little affected by  $nl$ , as expected for a parameter that has little effect on the restriction of the current-return path in the submyelin space. The Lillie transition gap giving rise to saltatory conduction ( $\delta_{salt}$ ) was somewhat smaller than  $\delta_{slow}$  and also unaffected by  $nl$ . Indeed for all  $nl$  examined (from 1 to 1000),  $\delta_{slow}$  varied from 2.0 to 1.6  $\mu\text{m}$  with  $\delta_{slow} = 1.6$  for  $nl > 37$  and  $\delta_{salt}$  was between 0.9 and 1.0  $\mu\text{m}$ . There was a small effect on the minimum conduction velocity (not visible at the scale shown in Fig. 3A2) ascribable to the decrease in permeability for sheaths having greater numbers of myelin layers. However, for  $\delta < \delta_{slow}$ , the speedup in conduction velocity with sheath tightening (decreasing  $\delta$ ) increased with higher  $nl$  values (Fig. 3A2). In this range of submyelin gaps ( $\delta < \delta_{slow}$ ), increasing  $nl$  caused an initially steep increase in conduction velocity, as shown in Fig. 3A3. This tapered off as the proportionate contribution to capacitance-reduction from each added layer decreased, approaching a maximum asymptotically as the number of layers approached infinity. The conduction velocity at the asymptote varied inversely with  $\delta$  (Fig. 3A3).

### 3.3 Slowdown, Lillie transition and rising phase are little affected by changes in node length

Figure 3 panels B1-B3 show analogous plots for the effects of changing the size of the node (“node length,”  $L_n$ ) on either side of its base value of 10  $\mu\text{m}$ . Changing node length changes the number of channels directly exposed to the external medium compared with the number of channels with that access reduced by current flow in the submyelin space. It also

## Transition to Saltatory Conduction

changes the membrane capacitance with direct access, in the same proportion. Figure 3B2 shows that  $L_n$  did not affect  $\delta_{salt}$ ,  $\delta_{slow}$ , or the magnitude of slowdown, since provided the internode was long compared to the node, overall external resistance with a loose sheath was dominated by the submyelin resistance, which in turn only depended on the submyelin gap. Indeed, throughout our  $L_n$  range of 0.001 to 20  $\mu\text{m}$ ,  $\delta_{slow}$  remained between 1.6 and 1.8  $\mu\text{m}$  and  $\delta_{salt}$  between 0.9 and 1.0  $\mu\text{m}$  (with  $\delta_{salt}$  always less than  $\delta_{slow}$ ). Furthermore, the slowdown from changing  $\delta = 10 \mu\text{m}$  to  $\delta_{slow}$  was 7.7 – 8% over our range of  $L_n$ . For  $\delta$  greater than 50 nm, changes in  $L_n$  within the range of 1 nm – 20  $\mu\text{m}$  yielded less than 0.18  $\text{m s}^{-1}$  variation in conduction velocity (Fig. 3B3, bottom three curves). At very small  $\delta$  ( $\delta \approx 1 \text{ nm}$ ; Fig. 3B3 top curve), a maximum conduction velocity of 9.4  $\text{m s}^{-1}$  occurred at around  $L_n = 10 \mu\text{m}$ , the value chosen for the base fiber. Shortening  $L_n$  below this value decreased conduction velocity by up to 10% for short nodes, an effect that was somewhat more pronounced with fewer myelin layers (not shown). Conduction velocity decreased as well (up to 4%) for  $L_n$  above 10  $\mu\text{m}$ , however this trend was not followed beyond  $L_n = 20 \mu\text{m}$ .

### 3.4 Slowdown and the Lillie transition are greatly affected by changes in internode length

Changing the internode length has several effects. It increases the resistance in the submyelin current-return path, but it provides greater “jump” distances for saltation between nodes, which if the current generated at a node has an ample safety factor, should speed a saltating impulse. Figure 3C1 shows that increasing the length of the internode covered by sheath,  $L_s$ , over the approximately 10-fold range from 250  $\mu\text{m}$  to 2250  $\mu\text{m}$  resulted in  $\delta_{slow}$  increasing from 0.2  $\mu\text{m}$  to a maximum of 1.8  $\mu\text{m}$ . The Lillie transition gap over this range shifted from  $\delta_{salt} = 0.1 \mu\text{m}$  to its maximum of 1.4  $\mu\text{m}$ , but was always smaller than  $\delta_{slow}$  (see Table 2). As  $L_s$  was increased beyond 2250  $\mu\text{m}$  up to 6000  $\mu\text{m}$ ,  $\delta_{slow}$  and  $\delta_{salt}$  reversed this progression, decreasing monotonically to 0.6  $\mu\text{m}$  and 0.5  $\mu\text{m}$ , respectively (Table 2). Throughout the range from  $250 \leq L_s \leq 6000 \mu\text{m}$  the minimum conduction velocity decreased monotonically with increasing  $L_s$  by 3% to 53% of the unmyelinated velocity, making an increasingly deep velocity trough prior to the onset of saltatory conduction, as would be expected from the lengthening of the restrictive submyelin space under pre-saltatory conditions (Fig. 3C2). The increase in conduction velocity for  $\delta < \delta_{slow}$  became more rapid as  $L_s$  increased, corresponding to an

## Transition to Saltatory Conduction

increasingly abrupt transition from slow continuous conduction to saltatory conduction. Note in Fig. 3C3 that for the gap of  $\delta = 0.5 \mu\text{m}$  (dark grey line with white dashes), lengthening  $L_s$  resulted in conduction velocity increasing to a maximum and then decreasing to less than the velocity for an unmyelinated axon in infinite medium, owing to the increasing load placed on the active node in charging the next increasingly distant distal node, ultimately resulting in failure of saltatory conduction. In general, for a sufficiently long internode, the loss of current reaching the next node will at some point be sufficient to cause failure of the saltatory mode at any gap size, leaving only the slow submyelin impulse propagating in a continuous mode.

### 3.5 Relative slowdown is less and speed up is greater for larger diameters

Axon core diameter has a well-known effect on impulse conduction velocity in both unmyelinated and myelinated nerve fibers. In the former case, the velocity varies as the square root of diameter, while for vertebrate fibers, in which myelin thickness and internode length also increase proportionately, the dependence is linear (e.g. Bullock and Horridge 1965). In our simulations, the myelin thickness was maintained fixed while diameter and  $\delta$  were varied. Increasing axon diameter across our range from 0.5 to 200  $\mu\text{m}$  increased  $\delta_{slow}$  from 0.03 to 6.0  $\mu\text{m}$  (see Fig. 3D1 white dots with black stars), with  $\delta_{salt}$  increasing as well, but in a proportion that dropped from  $\frac{3}{4}$  to about  $\frac{1}{2}$  of  $\delta_{slow}$  (Table 2). Since the conduction velocities are highly dependent on axon diameter for all values of  $\delta$ , it becomes difficult to determine which independent variable is responsible for conduction changes in Fig. 3D2. We address this issue by normalizing the curves in Fig. 3D2 with respect to the unmyelinated velocities such that, for each axon diameter, the velocity at  $\delta = 10 \mu\text{m}$  is redefined to be 1, and the resulting curves are plotted in the inset. Here, it is shown that for small diameter axons, tightening  $\delta$  results in a greater relative slowdown followed by a lesser relative speed up. The solid black line in Fig. 3D2 inset shows that for a diameter of 0.5  $\mu\text{m}$ , tightening  $\delta$  from 10  $\mu\text{m}$  to  $\delta_{slow}$  results a drop of 56% in conduction velocity. Furthermore, decreasing  $\delta$  from 10  $\mu\text{m}$  down to 1 nm increased conduction velocity by 461% for this same axon. However, when axon diameter is 200  $\mu\text{m}$  (white line with black dashes in Fig. 3D1 and 3D2), changing  $\delta$  over the same range resulted in a less than 1% drop in conduction velocity followed by a 536% increase. For each  $\delta$ , increasing axon diameter resulted in an increase in conduction velocity (see Fig. 3D3). This increase was

## Transition to Saltatory Conduction

proportional to the square root of the axon diameter for two  $\delta$  ranges: when the submyelin space was much larger than the diameter so the impulse propagation was continuous, and when the fiber was conducting well into the saltatory mode. In these two ranges, *conduction velocity* =  $K(\delta)(axon\ diameter)^{1/2}$ , where  $K(\delta)$  is constant for  $\delta \gg \delta_{slow}$  and inversely dependent on  $\delta$  for  $\delta \ll \delta_{slow}$ , for axon diameters down to those for which propagation times along the “node” become appreciable. Indeed, for our base axon diameter of 10.0  $\mu\text{m}$ ,  $K(\delta) = 548\ \text{m}^{1/2}\ \text{s}^{-1}$  for  $\delta = 10\ \mu\text{m}$  (black line with white dashes in Fig. 3D3) and  $K(\delta) = 2966\ \text{m}^{1/2}\ \text{s}^{-1}$  for  $\delta = 1\ \text{nm}$  (solid white line in Fig. 3D3).

### 3.6 The “Lillie transition” to saltatory conduction

Having examined the impact on conduction *velocity* of tightening the submyelin gap to induce saltatory conduction in an axon previously conducting only in continuous mode, we now examine the transition to the saltatory mode in more detail. Beginning with a loose sheath under which an impulse propagates in continuous mode, consider that as the sheath is tightened, the submyelin impulse travels progressively more slowly as the submyelin current-return resistance increases, a behavior that has been documented under different conditions above and is graphed with the solid curve in Fig. 4. Were there no “nodes” in the myelin, the conduction velocity would continue to drop as the gap narrows, decreasing with the square root of the submyelin cross sectional area, as shown by Lillie (1925) in the iron-wire model (shown as the dotted curve in Fig. 4). The *difference* between these two curves is plotted as the dashed curve, and represents the *added* velocity contributed by the nodes. Prior to the onset of saltatory conduction, the added velocity may be ascribed to the low-resistance current-return pathway provided by the nodes, which partially offset the sheath restriction. Saltatory conduction is characterized by a qualitative change in the mode of propagation as well as a quantitative increase in conduction speed. The transition gap width ( $\delta_{salt}$ ) is indicated by the vertical line with the circle symbol in Fig. 4. As described above, it is relatively independent of the number of myelin layers and node length ( $\delta_{salt} = 1.0\ \mu\text{m}$  for our base parameter set), but is dependent on internode length ( $L_s$ ) and diameter as enumerated in Table 2. In order to study the transition more closely, we monitored two voltages, one the trans-membrane (axolemma) voltage between axon interior and submyelin space (in the internodes), and the other the trans-fiber voltage from the interior to the exterior of

## Transition to Saltatory Conduction

the fiber including the myelin. Only in the former case is the impulse that travels under the myelin apparent. Figures 5A1 and 5B1 show respectively the trans-membrane and trans-fiber voltages for seven locations along an axon segment consisting of a 1500  $\mu\text{m}$  internode with two flanking nodes (i.e. having  $\sim 250$   $\mu\text{m}$  between recording sites) for a loose myelin sheath with  $\delta = 10$   $\mu\text{m}$ . The first (N1, lightest trace) and last (N2, darkest trace) spikes in each plot represent those at the nodes on either end of the internode. These spikes appear similar for either way of measuring voltage (Fig. 5A1 vs 5B1), with 150  $\mu\text{s}$  delays between successive longitudinal sites, reflecting the  $1.7 \text{ m s}^{-1}$  propagation speed of the spike in this standard 10  $\mu\text{m}$  axon. The trans-membrane voltage trajectories are almost exactly similar at each site, but displaced in time, while there is a slightly smaller amplitude measured for the trans-fiber voltages at the sites covered by myelin (traces S1-S5) due to the IR drop in the submyelin pathway accessing the extracellular points beneath the myelin. As the sheath is tightened to a 1  $\mu\text{m}$  gap (Fig. 5A2 and 5B2), the fiber begins to transition into saltatory mode. As defined in Methods, a saltatory mode is deemed to occur when a node “down stream” of an active node fires an impulse (i.e. reaches the criterion voltage  $V = 0$  mV) before the impulse traveling in the submyelin membrane arrives at that node. Skipping for the moment to a gap ( $\delta = 0.1$   $\mu\text{m}$ , Fig. 5A3 and 5B3) with clear saltatory conduction, Fig. 5A3 shows the spikes at the same seven monitoring sites as Fig. 5A1, with those at sites S1-S3 of the trans-membrane voltage representing the orthodromic propagation of the submyelin spike, occurring successively later, and those at sites S3-S5 successively earlier, representing the antidromic submyelin spike triggered by the earlier firing of the distal node (site N2), the two meeting and annihilating in mid-internode (site S3). The trans-fiber voltage, on the other hand (Fig. 5B3) is relatively little affected by what is transpiring under the myelin sheath. Rather, the voltage at each monitoring point, to a first approximation, represents the average of the voltage trajectories at the two nodes, weighted in inverse proportion to their distance from their respective node. The averaging is not strictly linear, however, as contributions are made by the submyelin membrane, attenuated by the restricted submyelin space. The situation for  $\delta = 0.01$   $\mu\text{m}$  is a more extreme version of the one just discussed (Fig. 5A4 and 5B4). Returning finally to the transitional case with  $\delta = 1.0$   $\mu\text{m}$  (Fig. 5A2 and 5B2), the submyelin spike (Fig. 5A2) occurs at successively later points along the internode, but the firing of the distal node (N2) occurs just barely later than the arrival time of the submyelin spike at S5 (voltage traces are almost superimposed at 0 mV). Hence, the distal node fires (reaches 0 mV) before the

## Transition to Saltatory Conduction

submyelin spike can propagate along the remaining 250  $\mu\text{m}$  of the internode to arrive at the node. Thus, by our criterion the fiber has transitioned to saltatory conduction. The trans-fiber waveforms are complex, but again can be seen as combinations of proportionate mixes of the wave forms at the two nodes. Returning for a moment to the conduction speed plot of Fig. 4, it should be noted that the  $\delta = 1.0 \mu\text{m}$  case just described corresponds to a point on the solid curve (overall conduction speed) where speed has already begun to increase above the minimum (at  $\delta_{slow} = 1.6 \mu\text{m}$ ) and the transition to saltation does not result in an abrupt change in the curve. This anticipatory speed increase may be ascribed in part, at least, to the assistance given by the distal node in a pre-saltatory state that still feeds current antidromically to enhance the submyelin impulse propagation.

Another instructive way to examine the transition to saltation is through plots of spike firing time (ordinate) vs position along the axon (abscissa) as shown in Fig. 6. To reiterate, the criterion for spike occurrence is the crossing of the 0 mV trans-membrane voltage, the results being slightly dependent on the choice of criterion. With a loose sheath ( $\delta = 10 \mu\text{m}$ ; Fig. 6A1 black curve), spike timing progresses smoothly and in monotonic linear fashion with distance along the fiber. The “nodes” are located at  $x = 0, 1500$  and  $3000 \mu\text{m}$  (indicated by filled circles). As the sheath is tightened ( $\delta = 1 \mu\text{m}$ ; Fig. 6A1 grey curve) overall propagation speed is slowed due the restriction in submyelin current return, but the transition to saltatory mode can be seen in the near simultaneous firing of each downstream node with the internodal membrane just preceding it. Note the upward bulge in the curve, as the impulse slows going into the internode and recedes farther from the low-resistance current-return access through the node, then speeds up as it reacquires that access approaching the more distal node. The slightly anticipated firing of the distal node isn’t sufficient to produce a noticeable region of negative slope on the curve at the distal ends of the internodes, but results in the curve flattening out. With further restriction to  $\delta = 0.1 \mu\text{m}$ , saltation has set in, with a clear local maximum in firing time for impulses arriving at the middle of the internode and a local minimum at the next distal node. The orthodromic conduction from the proximal node under the sheath is slower still (steeper slope), and when the distal node fires, it triggers a spike propagating antidromically under the sheath to meet and annihilate the orthodromically-propagating submyelin spike in the middle of the internode. Figure 6A2 shows this sequence more clearly for tighter sheaths and faster saltatory conduction,

## Transition to Saltatory Conduction

the pre-saltatory curve (black line) showing the linear progression of nearly constant-velocity continuous submyelin conduction with a loose sheath, and the progressively earlier nodal firing (at  $x = 1500$  and  $3000 \mu\text{m}$ ), and the antidromic mode creating the triangular plots for  $\delta = 0.1$  and  $0.01 \mu\text{m}$ . Figure 6B shows similar plots for the trans-fiber impulse. With a loose sheath ( $\delta = 10 \mu\text{m}$ ) spike times increase linearly with distance along the fiber. In the transitional case ( $\delta = 1 \mu\text{m}$ ), which can perhaps be best appreciated by referring to Fig. 5B2, the spike trajectory in the internode near the proximal node is dominated by the spike being generated at the node, so it reaches the criterion of 0 mV earlier than with a looser sheath, giving an appearance of a speed up in the plot. This is soon reversed as the trans-fiber spike becomes more strongly influenced by the more delayed spike at the distal node, producing an appearance of a slowdown, and finally a flattening of the curve (meaning a near-synchrony of firing at adjacent trans-fiber locations) at positions near the distal node. This irregularity in apparent spike timing smooths out progressively as the sheath is further tightened to  $\delta = 0.1 \mu\text{m}$  and then  $0.01 \mu\text{m}$  (Fig. 6B, curve with white circles).

## 4 Discussion

We have examined theoretically the experiments of Lillie (1925) demonstrating that by insulating short segments of an active core conductor one can achieve a more rapid saltatory mode of impulse conduction. This we have done using the more physiologically realistic formulation for nerve impulse conduction developed by Hodgkin and Huxley in 1952, helping bridge Lillie's original studies to the issues of the evolution and development of myelin under biological constraints. In charting the behavior of an unmyelinated axon as a capacitance-lowering sheath, punctuated by nodes, is progressively tightened, we find that the "Lillie" transition to saltatory conduction occurs for surprisingly loose ensheathments, with gaps only about one order of magnitude smaller than the axonal diameter, given other parameters not excessively far from those found in nature. Lillie's original observations demonstrated that the specialized paranodal seals between myelin and axon isolating the nodal membrane from internodal membrane in the submyelin space are not prerequisites for saltatory conduction. Our results confirm this observation using a more "realistic" axonal core. Lillie's observations also showed that even the clustering of sodium channels at the nodes is not necessary for saltatory



## Transition to Saltatory Conduction

conduction, which again we confirm with the squid core (see also Hartline 2008). In particular, a gap corresponding to the normal intercellular distance between axolemma and the surrounding glia (ca 10-20 nm in fixed material) is the transition point for an axon of 0.5  $\mu\text{m}$  diameter with uniformly-distributed squid density channels, interestingly close to the minimum size of a myelinated vertebrate axon. Thus the conditions for achieving saltatory conduction are surprisingly permissive.

### 4.1 Model behavior

The primary parameter varied in our studies was the submyelin gap – the “tightness” of the sheath, and this was the most critical factor in determining the transition to saltatory conduction. Decreasing the size of this gap raises the resistance of the current loops traveling in advance of the continuously-conducting submyelin impulse, which slows its conduction velocity. The effect is equivalent to that of decreasing the axon diameter, which thereby restricts the internal axial resistance. As Lillie (1925) determined, this caused a slow-down of conduction, and indeed, he demonstrated the square root relationship between sub “myelin” conductivity and conduction velocity, which relationship can be noted for the positive slopes of the firing time vs position curves in the internodal regions of Fig. 6A1-A2. In the saltatory range, the persistence of conduction velocity increases with sheath tightening, even to unnaturally-small gaps (e.g. 0.1 nm) may be ascribed to the decreasing access of nodal current to the capacitance-increasing paranodal regions, in effect mimicking the effects of septate junctions of the paranodal endloops in vertebrate nodes.

Our model’s behavior with varying myelin parameters other than sheath tightness qualitatively paralleled what has been documented by others in simulating tightly-sheathed axons, suggesting that the qualitative dependence of conduction velocity on parameters of fiber geometry is quite robust. Effects of changing the number of layers ( $nl$ ) in the sheath on conduction velocity arise from changing both the resistive (“leak”) and capacitive components of insulation. Our results agree well with those of previous studies, in which external fiber diameter was allowed to vary along with sheath thickness (Smith and Koles 1970; Moore *et al.* 1978; Chomiak and Hu 2009). In particular, we found that conduction velocity was a

## Transition to Saltatory Conduction

monotonically increasing function of sheath thickness that saturates for large numbers of layers (Fig. 3A3, white line) similar to that described by Smith and Koles (1970). This is consistent with the observation of Moore *et al.* (1978) that for their parameter set, increasing the number of myelin layers had a proportionally smaller effect on conduction velocity than decreasing myelin specific capacitance. The rate at which conduction velocity saturates with increasing  $nl$  depends on the tightness of the sheath ( $\delta$ ), with tighter sheaths saturating at larger  $nl$  and correspondingly higher conduction velocities. The effects of node length ( $L_n$ ) on conduction velocity in the saltatory range were modest, with a broad peak at a node length that shifted to larger  $L_n$  with increasing gap size. These effects were similar to those studied by Moore *et al.* (1978), who separated out the effects of changing node capacitance alone from changing node area while maintaining constant channel density. They made the interesting observation that for the parameter set used in their model, the effects on conduction velocity of changing capacitance and changing the number of channels in the same proportion tended to cancel. In our model, the contribution of the standard 10  $\mu\text{m}$  long node to the overall capacitance of each node-internode segment is nearly equal to that of the 1500  $\mu\text{m}$  internode with 100 double layers of myelin ( $10: [1500/201] = 1.3$ ; this proportion was 0.32 for Moore *et al.* 1978). As  $L_n$  is decreased, this proportion decreases, hence the positive effect its reduction has on conduction velocity is lessened relative to the negative effect of decreasing the number of channels carrying current, which dominates for very short nodes (Fig. 3B3, white line). Increasing  $L_n$  tends in the opposite direction, increasing the influence of capacitive changes on conduction velocity (Fig. 3B3). The effect that changing the internode length ( $L_s$ ) has on conduction velocity has been examined by Brill *et al.* (1977) for a wide range of internode lengths. They found that conduction velocity was very sensitive to  $L_s$  for short internodes, reached a broad peak at intermediate lengths followed by a gradual decrease and finally the failure of impulse propagation at very long internodes. Conduction velocity showed a similar pattern of dependence on  $L_s$  for our model, although impulse conduction didn't fail at long internodes because of the presence of a submyelin impulse, but instead transitioned back to continuous conduction. This can be seen in Fig. 3C1 and 3C3 for the relatively large submyelin space of  $\delta = 0.5$  (dark grey line with white dashes) in which the conduction velocity increased and then decreased as the mode of impulse conduction passed from continuous to saltatory and back to continuous as  $L_s$  was increased. For tighter sheaths ( $\delta < 0.5$ ), the transition back to continuous conduction from saltatory conduction

## Transition to Saltatory Conduction

was shifted to larger internode lengths as was the peak conduction velocity (not shown). For tight sheaths, conduction velocity increased approximately as  $L_s^{1/2}$  for  $250\mu\text{m} < L_s < 1500\mu\text{m}$ . This dependence on  $L_s$  decreased gradually as the sheath was loosened ( $\delta$  increased). Diameter has a well known-effect on conduction velocity owing to its modification of the internal axoplasmic resistance per unit length. For unmyelinated fibers it has a square root dependency (Pumphrey and Young 1938), whereas the normal dependency for myelinated fibers is linear. As pointed out by Goldman and Albus (1968) the difference arises because the myelin sheath of vertebrate axons typically thickens in proportion to the fiber diameter, to maintain a constant ratio of inner (axonal) to fiber (including sheath) diameter. The square root relation in our axons was owing to holding the sheath thickness fixed as the diameter was varied (Fig. 3D3).

### 4.2 Lillie transition

Several points should be noted about the transition to saltatory conduction that are largely independent of the values of parameters such as diameter, number of layers and node length. First, there is not a discontinuous jump in conduction velocity that corresponds to the onset of saltation. Saltation as we have defined it occurs when a more distal node fires before arrival of the impulse traveling in the submyelin space. This is a distinct point in parameter space, yet it is a smooth transition in the dependence of conduction velocity on the parameters. In fact, as shown clearly in Fig. 4 (vertical lines), conduction velocity as a function of decreasing  $\delta$  reaches a minimum and starts creeping up even before the onset of saltation. This is because the voltage at the distal node, being brought to near threshold by current spreading from the proximal node, is augmented by the advancing depolarization spreading ahead of the submyelin impulse, which thereby brings the node to threshold sooner. Thus, in the model we have studied, with a high density of sodium channels under the myelin, the continuously-propagating submyelin impulse aids in smoothing the transition to saltation. Over most of the parameter range that we examined, the transition to saltation occurs even before the conduction velocity has returned to that of the unmyelinated axon (Fig. 4, vertical lines with circle and square, respectively). Hence, the transition to saltatory conduction doesn't in itself result in an increase in conduction velocity beyond that of the unmyelinated axon (or in other words, the model allows for slow saltatory conduction).

## Transition to Saltatory Conduction

The transition to saltatory mode nevertheless exhibits different levels of abruptness depending on parameters. This is particularly evident for very long internode lengths ( $L_s$ ). During normal saltatory conduction (and this includes biologically-observed cases), calculations from conduction speed and internode lengths reveal that several adjacent nodes participate simultaneously in generating the impulse, albeit at different phases. This shows clearly in the piecewise linearity of the impulse shown in Fig. 2's upper inset, in which five "active" nodes are at voltages exceeding the 0 mV impulse criterion level, spanning a time interval of *ca* 1.2 ms. Provided impulse amplitude is unchanged, this interval of 1.2 ms is independent of conduction velocity. Thus, if node spacing is kept constant, the number of active nodes decreases with decreasing conduction speed. For internode length, on the other hand, the number of active nodes decreases as  $L_s$  is increased *despite* increases in conduction speed (for example from Fig. 3C3 for  $\delta = 0.01 \mu\text{m}$ , conduction speeds at  $L_s = 1, 3$  and  $5 \text{ mm}$  are  $6, 8.3$  and  $9.6 \text{ m s}^{-1}$  respectively, but the 1.2 ms time-span with  $V_m > 0 \text{ mV}$  involves 7.2, 3.3 and 2.3 nodes respectively). When this active node number, for whatever reason, drops below 1.0, a condition occurs that might be termed "eusaltatory conduction" in which only one node at a time "fires" (i.e. has  $V_m > 0 \text{ mV}$ ) and the impulse truly "jumps" from node to node. If parameters are changed too much more in the same direction, the safety factor for impulse generation becomes too small and the impulse will fail, as the current generated by a more proximal node is insufficient to reach firing threshold at the more distal node. This perspective looks at the transition to saltation a little differently: what conditions are required to bring the distal node to threshold? For parameter values in the neighborhood of a low safety factor, conditions at an inactive node hover near firing during the development of the local response (Hodgkin 1938). A small change in a parameter will then have a relatively large effect on determining whether or not the node fires, yielding a faster (saltatory) or slower (non-saltatory) conduction velocity. This appears to explain the more abrupt transitions obtained for some of the parameters we explored (e.g. Figs. 3C1, 3C2, 3D2 inset).

## Transition to Saltatory Conduction

### 4.3 Sheath-tightening as a mechanism in myelin evolution

If we hypothesize that the increased velocity and decreased metabolic cost of saltatory conduction provide a driving force for myelin evolution, then the above results suggest that a possible mechanism for myelin evolution might proceed by tightening short segments of membranous sheath, such as the cell membrane of surrounding glia, around a large diameter axon to form short internodes. Once the sheath is tight enough for the transition to saltatory conduction ( $\delta < \delta_{salt}$ ) to occur, myelination can continue by elongating internodes and adding more layers of membrane to further increase conduction velocity. For example, if an insulating sheath of length  $L_s = 250 \mu\text{m}$  tightens to within the observed physiological range for the submyelin space e.g.  $\delta = 0.01 \mu\text{m}$  (see Fig. 3C1, C2, solid black line) and then elongates (Fig. 3C1, light gray dotted line), the conduction velocity undergoes only a minor slowdown. The slowdown represents an “energy barrier” to the evolution of myelin, and hence, a potential evolutionary pathway must minimize the slowdown. In addition, if the myelinating axon has a sufficiently large diameter (see Fig. 3D2 inset, grey dotted line, diameter  $\geq 10 \mu\text{m}$ ), then the conduction velocity experiences only a minimal slowdown as the sheath is tightened. Hence, this barrier is smaller for larger axons, which may help explain the preferential myelination of large axons actually observed.

### 4.4 Conclusions

The ground-breaking insight and experiments of Lillie’s demonstrated dramatically the potential impact on nerve conduction mode of installing an insulating sheath, punctuated by openings, around a continuously conducting axon. The studies we have presented examine the parametric dependence of this “Lillie transition” from continuous to saltatory conduction. Up to a point, this dependence may be useful in understanding evolutionary and developmental steps in producing saltatory conduction. It shows that neither paranodal sealing nor channel clustering are absolute requirements for saltatory conduction. However, it remains unrealistic in that it has utilized a fully-formed insulating sheath that is tightened around a fully conducting axon. These latter features remain to be investigated more fully in understanding the transition to saltatory conduction.

### **Acknowledgments**

We thank Drs. Michael Hines and Ted Carnevale for providing the NEURON simulation software, and Drs. Andrew Christie and Petra Lenz for valuable criticism of earlier drafts. We are very appreciative of support provided by the National Science Foundation (Interdisciplinary Training for Undergraduates in Biological and Mathematical Science award NSF DUE-0634624, and NSF IOS-0923692), and The Cades Foundation, Honolulu, HI.

## Transition to Saltatory Conduction

Table 1 Parameter values and ranges

Parameter	Base value	Tested range
Submyelin gap ( $\delta$ )	–	0.001 – 100 $\mu\text{m}^{\text{a}}$
Number of myelin wraps ( $nl$ )	100	1 – 1000
Node length ( $L_n$ )	10 $\mu\text{m}$	0.001 – 20 $\mu\text{m}$
Internode length ( $L_s$ )	1500 $\mu\text{m}$	250 – 6000 $\mu\text{m}$
Axon diameter	10 $\mu\text{m}$	0.5 – 200 $\mu\text{m}$

a. For some runs (e.g. those examining the effects of axon diameter), the  $\delta$  range was extended to  $10^{-6}$  -  $10^3 \mu\text{m}$ .

## Transition to Saltatory Conduction

Table 2 Submyelin gap ( $\delta$ ) at slowest velocity ( $\delta_{slow}$ ) and transition to saltation ( $\delta_{salt}$ ) for internode length ( $L_s$ ) and axon diameter. The values of  $\delta_{slow}$  and  $\delta_{salt}$  were almost independent of  $L_n$  and  $nl$

Parameter-multiplier	$L_s: 1500\mu\text{m}^a$		$Diameter: 10\mu\text{m}^a$	
	$\delta_{slow} (\mu\text{m})$	$\delta_{salt} (\mu\text{m})$	$\delta_{slow} (\mu\text{m})$	$\delta_{salt} (\mu\text{m})$
0.1	0.09	0.05	0.07	0.05
0.5	1.0	0.45	0.90	0.70
1.0	1.6	1.0	1.6	1.0
2.0	1.6	1.2	2.8	1.4
4.0	0.6	0.5	4.0	1.8

a. Base value of the parameter being varied ( $L_s$  or  $diameter$ ) corresponding to the multiplier 1.0. In each case, all other parameters had their base values (see Table 1).



## Figure captions

### Fig. 1

Axon model diagram and equivalent circuit. (A) Diagram of the model axon showing the parameters that describe the variable sheath geometry. The submyelin gap  $\delta$ , number of myelin wraps  $nl$ , node length  $L_n$ , internode length  $L_s$ , and axon diameter are varied over the parameter ranges given in Table 1. (B) Equivalent circuit of A. The circuitry of the axolemma represents the Hodgkin-Huxley model of a squid axon and is labeled  $R_m$  and  $C_m$  for the membrane resistance and capacitance, respectively. The axoplasmic resistivity is given by  $R_i$ . The parameters  $R_s$  and  $C_s$  represent the resistance and capacitance of the sheath, respectively, and are proportional and inversely proportional to the number of wraps,  $nl$  ( $1/R_s = (10^{-6})/(2nl) \Omega \text{ cm}^2$  and  $C_s = 1/(2nl) \mu\text{F cm}^2$ ).  $R_o$  is the longitudinal resistance of the submyelin space and is set to  $35.6/A \Omega \text{ cm}$ , where  $A$  is the cross-sectional area in  $\text{cm}^2$  of the submyelin space

### Fig. 2

Model behavior. Dependence of conduction velocity on width of submyelin space,  $\delta$ , for model with “base” parameter values (Table 1). The model is shown at the “base” temperature of 6.3 °C (black line), and two additional temperatures of 10.0 °C and 15.0 °C for comparison (gray lines). For all three temperatures, conduction velocities slow down to a minimum and then speed up as  $\delta$  decreases. (Insets) Signal propagation of trans-fiber voltage (outside of “sheath” minus inside of axon) vs distance along axon at three time increments ( $\Delta t = 1.25 \text{ ms}$  apart) for two submyelin gap sizes (indicated by arrows). Time intervals are referenced to the time when the impulse leading edge crosses 0 mV. Positions are given relative to the center of a node (defined to be at 0 mm) sufficiently distant from the ends of the axon. (Lower inset) Continuous conduction for a submyelin gap of 10  $\mu\text{m}$ . (Upper inset) Tightening the gap to 0.01  $\mu\text{m}$  induces saltatory conduction with early nodal firing. Note the piecewise linear drop of voltage from node to node (node positions visible as “corners” in the waveform at 1.5 mm intervals) in contrast to the smooth progression of voltage in continuous conduction and the lower amplitude owing to participation of fewer channels in generating the current

**Fig. 3**

Dependence of the relationship between conduction velocity and submyelin gap,  $\delta$ , on the following myelin sheath parameters: number of myelin wraps,  $nl$ , (A1-A3); node length,  $L_n$ , (B1-B3); internode length,  $L_s$ , (C1-C3), and axon diameter (D1-D3). The 3D plots (A1, B1, C1, and D1) show conduction velocity ( $v$ , z-axis) vs submyelin gap size ( $\delta$ , x-axis) and the parameter under study (y-axis). The patterned lines on each 3D plot correspond to the equivalently patterned lines on the 2D plots of the same row. The first of each pair of 2D plots (A2, B2, C2, and D2) shows conduction velocity vs submyelin gap for select values of the parameter under study (key directly to the right of the panels), while the second of each pair (A3, B3, C3, and D3) shows conduction velocity vs the parameter under study for select submyelin gaps (see key at the upper right). Note that lines for  $\delta = 10$  and  $\delta = 5$  superimpose in the right-most panels. The inset of D2 shows the plot of normalized conduction velocity ( $NCV$ ) vs submyelin gap for the same axon diameters. Here, the curves are normalized to the unmyelinated velocity (at  $\delta = 10 \mu\text{m}$ ) for each diameter

**Fig. 4**

Transition to saltatory conduction. Plots of the difference in the conduction speed from that of an unmyelinated axon ( $\delta \geq 10 \mu\text{m}$ , grey horizontal line) as a function of sheath tightness ( $\delta$ ) showing the net conduction velocity (solid line), the slowdown in velocity due just to the increased external resistance of the submyelin space (dotted line), and the difference between the two, representing the increase in velocity due to the presence of nodes and the transition to saltatory conduction (dashed line). The vertical lines represent:  $\delta_{slow} = 1.6 \mu\text{m}$ , the gap size with the slowest conduction velocity (right, triangle),  $\delta_{salt} = 1.0 \mu\text{m}$ , the largest gap size sustaining saltation (middle, circle) and  $\delta = 0.75 \mu\text{m}$ , the gap size for which the conduction velocity equals that of the unmyelinated axon (left, square)

**Fig. 5**

Comparison between trans-membrane and trans-fiber voltages as the myelin sheath is tightened. Upper diagram shows the trans-membrane (from the axoplasm to the submyelin space) and the trans-fiber (from the axoplasm to the external medium) voltage drops, and the positions along the axon corresponding to the voltage traces below. (A) Trans-membrane voltage for different

## Transition to Saltatory Conduction

submyelin gaps ( $\delta = 10, 1, 0.1, \text{ and } 0.01 \mu\text{m}$  for subpanels numbered A1 through A4). The action potentials are shown as functions of time for the center of a node (N1), 5 equally spaced positions along the internode (S1 through S5) and the center of the next more distal node (N2). (B1-B4) Trans-fiber voltage for the same positions along the axon and the same submyelin gaps as in A

### **Fig. 6**

Firing times as a function of position for selected submyelin gap sizes. (A1-A2) Firing times are defined to be the time when the trans-membrane (cf. trans-fiber) voltage crosses  $V = 0 \text{ mV}$  in the positive direction (interpolated from two adjacent points on the voltage-trajectory) for different locations along the axon (abscissa). Measurements are given relative to the firing time (defined to be 0 ms) at the center of an arbitrary node (defined to be at  $0 \mu\text{m}$ ) sufficiently distant from the ends of the axon. Nodes occur at multiples of  $1500 \mu\text{m}$  and are indicated by shaded circles on the curves. From the darkest to the lightest shade, each line and circle corresponds to a different gap size with  $\delta = 10$  (black line and circle), 1, 0.1, and  $0.01 \mu\text{m}$  (white line and circle). A curve with a region of negative slope (implying that distal [nodal] membrane reaches  $V = 0$  before proximal [internodal] membrane) indicates saltatory conduction (e.g.  $\delta = 0.1$  curve). A1 and A2 differ only in ordinate scales. The timing of the submyelin impulses for  $\delta = 0.1, 0.01$  and  $0.001$  (not shown) have constant slopes distant from the nodes, representing uniform velocities of  $0.36, 0.11$  and  $0.036 \text{ m s}^{-1}$  respectively, which obey an (approximate)  $\delta^{1/2}$  relation. (B) Similar firing times based on trans-fiber voltage crossing of  $V = 0 \text{ mV}$ . See text for description

## References

- Brill, M. H., Waxman, S. D., Moore, J. W. & Joyner, R. W. (1977). Conduction velocity and spike configuration in myelinated fibres: computed dependence on internode distance. *Journal of Neurology, Neurosurgery and Psychiatry*, **40**, 769-774.
- Brösamle, C. & Halpern, M. E. (2002). Characterization of myelination in the developing zebrafish. *Glia*, **39**, 47-57.
- Bullock, T. H. & Horridge, G. A. (1965). *Structure and Function in the Nervous System of Invertebrates.*, vol. 1. San Francisco: W. H. Freeman.
- Calvin, W. H. & Hartline, D. K. (1977). Retrograde invasion of lobster stretch receptor somata in control of firing rate and extra spike patterning. *Journal of Neurophysiology*, **40**, 106-118.
- Carnevale, N. T. & Hines, M. L. (2005). *The NEURON Book*. Cambridge, U.K.: Cambridge University Press.
- Carpenter, F. G. & Bergland, R. M. (1975). Excitation and conduction in immature nerve fibers of the developing chick. *American Journal of Physiology*, **190**, 371-376.
- Chomiak, T. & Hu, B. (2009). What is the optimal value of the g-ratio for myelinated fibers in the rat CNS? A theoretical approach. *PLoS One*, **4**, e7754.
- Foster, R. E., Connors, B. W. & Waxman, S. D. (1982). Rat optic nerve: electrophysiological, pharmacological and anatomical studies during development. *Brain Research*, **255**, 371-386.
- Freidländer, B. (1889). Über die markhaltigen Nervenfasern und Neurochorde der Crustaceen und Anneliden. *Mittheilungen aus der Zoologischen Station zu Neapel*, **9**, 205-265.
- Goldman, L. & Albus, J. S. (1968). Computation of impulse conduction in myelinated fibers: Theoretical basis of the velocity-diameter relation. *Biophysical Journal*, **8**, 596-607.
- Goldstein, S. S. & Rall, W. (1974). Changes of action potential shape and velocity for changing core conductor geometry. *Biophysical Journal*, **14**, 731-757.
- Halter, J. A. & Clark, J. W. (1991). A distributed-parameter model of the myelinated nerve fiber. *Journal of Theoretical Biology*, **148**, 345-382.
- Hartline, D. K. (2008). What is myelin? *Neuron Glia Biology*, **4**, 153-163.
- Hartline, D. K. & Colman D.R. (2007). Rapid conduction and the evolution of giant axons and myelinated fibers. *Current Biology*, **17**, R29-R35.

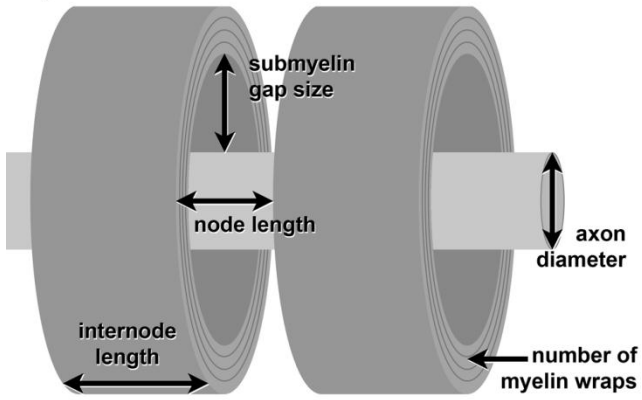
## Transition to Saltatory Conduction

- Hille, B. (1992). *Ionic Channels of Excitable Membranes*, Second edn. Sunderland, MA: Sinauer Associates Inc.
- Hines, M. L. & Shrager, P. (1991). A computational test of the requirements for conduction in demyelinated axons. *Restorative Neurology, and Neuroscience*, **3**, 81-93.
- Hodgkin, A. L. (1938). The subthreshold potentials in a crustacean nerve fibre. *Proceedings of the Royal Society of London Series B*, **126**, 87-121.
- Hodgkin, A. L. & Huxley, A. F. (1952). A quantitative description of membrane current and its application to conduction and excitation in nerve. *Journal of Physiology*, **117**, 500-544.
- Huxley, A. F. & Stämpfli, R. (1949). Evidence for saltatory conduction in peripheral myelinated nerve fibers. *Journal of Physiology*, **108**, 315-339.
- Lillie, R. S. (1925). Factors affecting transmission and recovery in the passive iron nerve model. *Journal of General Physiology*, **7**, 473-507.
- Moore, J. W., Joyner, R. W., Brill, M. H., Waxman, S. D. & Najar-Joa, M. (1978). Simulations of conduction in uniform myelinated fibers: Relative sensitivity to changes in nodal and internodal parameters. *Biophysical Journal*, **21**, 147-160.
- Pumphrey, R. J. & Young, J. Z. (1938). The rates of conduction of nerve fibres of various diameters in cephalopods. *The Journal of Experimental Biology*, **15**, 453-466.
- Raine, C. (1984). Morphology of myelin and myelination. In P. Morell (Ed.), *Myelin*, second edn, (pp. 1-50). London: Plenum Press.
- Rovainen, C. M. (1967). Physiological and anatomical studies on large neurons of central nervous system of the sea lamprey (*Petromyzon marinus*). I. Müller and Mauthner cells. *Journal of Neurophysiology*, **30**, 1000-1023.
- Seidl, A. H., Rubel, E. W. & Harris, D. M. (2010). Mechanisms for adjusting interaural time differences to achieve binaural coincidence detection. *Journal of Neuroscience*, **30**, 70-80.
- Smith, R. S. & Koles, Z. J. (1970). Myelinated nerve fibers: computed effect of myelin thickness on conduction velocity. *American Journal of Physiology*, **219**, 1256-1258.
- Tasaki, I. (1939). The electro-saltatory transmission of the nerve impulse and the effect of narcosis upon the nerve fiber. *American Journal of Physiology*, **127**, 211-227.
- Vabnick, I. & Shrager, P. (1999). Ion channel redistribution and function during development of the myelinated axon. *Journal of Neurobiology*, **37**, 80-96.

## Transition to Saltatory Conduction

- Wilson, C. H. & Hartline, D. K. (2011). Novel organization and development of copepod myelin. I. Ontogeny. *Journal of Comparative Neurology*, **519**, 3259-3280.
- Xu, K., Sun, H. & Sung, Y. (1994). Electron microscopic observation on ontogenesis of the myelinated nerve fiber in the shrimp (*Panaeus orientalis*). *Chinese Journal of Neuroanatomy*, **10**, 239-241.
- Zalc, B., Goujet, D. & Colman, D. R. (2008). The origin of the myelination program in vertebrates. *Current Biology*, **18**, R511-R512.

A)



B)

